



HAL
open science

North Pacific atmospheric rivers and their influence on western North America at the Last Glacial Maximum

Juan M. Lora, Jonathan L. Mitchell, Camille Risi, Aradhna E. Tripati

► **To cite this version:**

Juan M. Lora, Jonathan L. Mitchell, Camille Risi, Aradhna E. Tripati. North Pacific atmospheric rivers and their influence on western North America at the Last Glacial Maximum. *Geophysical Research Letters*, 2017, 44, pp.1051-1059. 10.1002/2016GL071541 . insu-03727088

HAL Id: insu-03727088

<https://insu.hal.science/insu-03727088>

Submitted on 21 Jul 2022

HAL is a multi-disciplinary open access archive for the deposit and dissemination of scientific research documents, whether they are published or not. The documents may come from teaching and research institutions in France or abroad, or from public or private research centers.

L'archive ouverte pluridisciplinaire **HAL**, est destinée au dépôt et à la diffusion de documents scientifiques de niveau recherche, publiés ou non, émanant des établissements d'enseignement et de recherche français ou étrangers, des laboratoires publics ou privés.

Copyright



RESEARCH LETTER

10.1002/2016GL071541

Key Points:

- Atmospheric rivers at the Last Glacial Maximum were shifted southeast and increased southwesterly moisture transport to southwestern North America
- Model-data comparisons show higher model skills in models that simulate more southeasterly changes near the North American coast
- Magnitude of precipitation differences due to atmospheric rivers are consistent with reconstructed regional patterns

Supporting Information:

- Supporting Information S1

Correspondence to:

J. M. Lora,
jlora@ucla.edu

Citation:

Lora, J. M., J. L. Mitchell, C. Risi, and A. E. Tripati (2017), North Pacific atmospheric rivers and their influence on western North America at the Last Glacial Maximum, *Geophys. Res. Lett.*, *44*, 1051–1059, doi:10.1002/2016GL071541.

Received 10 OCT 2016

Accepted 30 DEC 2016

Accepted article online 5 JAN 2017

Published online 30 JAN 2017

North Pacific atmospheric rivers and their influence on western North America at the Last Glacial Maximum

Juan M. Lora¹ , Jonathan L. Mitchell^{1,2,3}, Camille Risi⁴ , and Aradhna E. Tripati^{1,3,5,6}

¹Department of Earth, Planetary, and Space Sciences, University of California, Los Angeles, California, USA, ²Department of Physics, Westmont College, Santa Barbara, California, USA, ³Department of Atmospheric and Oceanic Sciences, University of California, Los Angeles, California, USA, ⁴Laboratoire de Météorologie Dynamique, CNRS, Paris, France, ⁵Institute of the Environment and Sustainability, University of California, Los Angeles, California, USA, ⁶European Institute of Marine Studies, University of Western Brittany (UBO), Plouzané, France

Abstract Southwestern North America was wetter than present during the Last Glacial Maximum. The causes of increased water availability have been recently debated, and quantitative precipitation reconstructions have been underutilized in model-data comparisons. We investigate the climatological response of North Pacific atmospheric rivers to the glacial climate using model simulations and paleoclimate reconstructions. Atmospheric moisture transport due to these features shifted toward the southeast relative to modern. Enhanced southwesterly moisture delivery between Hawaii and California increased precipitation in the southwest while decreasing it in the Pacific Northwest, in agreement with reconstructions. Coupled climate models that are best able to reproduce reconstructed precipitation changes simulate decreases in sea level pressure across the eastern North Pacific and show the strongest southeastward shifts of moisture transport relative to a modern climate. Precipitation increases of $\sim 1 \text{ mm d}^{-1}$, due largely to atmospheric rivers, are of the right magnitude to account for reconstructed pluvial conditions in parts of southwestern North America during the Last Glacial Maximum.

1. Introduction

During the glacial stages of the Pleistocene, the now-arid southwestern North America was much wetter than present [COHMAP Members, 1988; Oviatt et al., 1999; Lyle et al., 2012]. A prime example is the presence of pluvial lakes of considerable size during the Last Glacial Maximum (LGM; ~ 23 – 19 ka) extending from the Great Basin to southern California [Benson et al., 2011; Reheis et al., 2012; Kirby et al., 2013]. Climate estimates from paleo-vegetation data [Thompson et al., 1999; Bartlein et al., 2011] and various other sources [Lemons et al., 1996; Owen et al., 2003; Wagner et al., 2010; Ibarra et al., 2014; Maher et al., 2014; Lachniet et al., 2014] similarly indicate higher mean annual precipitation across the southwest during the LGM.

The causes of these increases in water availability and the source of precipitation feeding the region are debated. A leading hypothesis is a southward shift of the storm track toward the southwest as a result of the midlatitude jet being split or shifted south by the large North American ice sheets during glacial intervals [Kutzbach and Wright, 1985; Manabe and Broccoli, 1985; COHMAP Members, 1988; Hostetler and Benson, 1990; Bartlein et al., 1998; Bromwich et al., 2004; Kim et al., 2008; Kirby et al., 2013]. Additional hypotheses include a substantially enhanced North American Monsoon [Lyle et al., 2012] or that the storm track was routed in a northwesterly trajectory across the western United States by strengthened high-pressure systems over the eastern North Pacific and the continent [Oster et al., 2015].

Here we explore North Pacific atmospheric rivers (ARs) and their role in transporting moisture to different regions of western North America during the LGM. Modern ARs constitute an essential mechanism of water delivery to the continent [Ralph et al., 2006; Neiman et al., 2008; Guan et al., 2010; Dettinger et al., 2011]. These plumelike features of the extratropical atmosphere are long and narrow conduits of atmospheric moisture that account for the vast majority (upward of 90%) of poleward moisture transport outside of the tropics [Zhu and Newell, 1998]. ARs cause substantial precipitation in short-lived events that can produce torrential rainfall and severe flooding [Ralph et al., 2005, 2006; Neiman et al., 2008; Knipperz and Wernli, 2010; Dettinger et al., 2011; Ralph et al., 2011; Hendy et al., 2015], and they are responsible for considerable

fractions—up to 50%—of total rainfall in modern California and the Pacific Northwest [Guan *et al.*, 2010; Dettinger *et al.*, 2011], and 15%–40% in the southwest [Rutz and Steenburgh, 2012]. These filaments of focused water vapor content are dynamically related to moisture convergence in the warm conveyor belts ahead of extratropical cyclones, but they are distinct features that can be associated with multiple cyclonic systems and undergo unique life cycles [Cordeira *et al.*, 2013; Sodemann and Stohl, 2013; Payne and Magnusdottir, 2014; Mundhenk *et al.*, 2016]. ARs extend from the (sub)tropics, and incorporate moisture from remote tropical and subtropical, as well as local, source regions into the extratropics [Bao *et al.*, 2006; Knipperz and Wernli, 2010; Cordeira *et al.*, 2013; Sodemann and Stohl, 2013; Dacre *et al.*, 2015]. Yet despite their importance to the modern water budget of western North America, the behavior of ARs in the North Pacific during the LGM has not been systematically studied.

2. Modern Climate From Reanalysis

Most precipitation in western North America associated with ARs occurs during the cold season [Neiman *et al.*, 2008; Knipperz and Wernli, 2010; Rutz *et al.*, 2014; Payne and Magnusdottir, 2014], so we examine vapor transport and precipitation during the winter half year (October–March) as a baseline modern climatology for further comparisons. We employ atmospheric variables from the National Aeronautics and Space Administration's Modern-Era Retrospective Analysis for Research and Applications 2 (MERRA-2) reanalysis for the years 1981–2010. From this data set we also identify ARs based on vertically integrated vapor transport (IVT; supporting information) and quantify their direct climatological contributions to IVT and precipitation.

Climatological cold-season IVT occurs across the North Pacific, with southwesterly transport (exceeding $200 \text{ kg m}^{-1} \text{ s}^{-1}$) extending from around 160°W to the North American continent (Figure 1a). The mean precipitation distribution for the same season closely corresponds to this layout, peaking around 10 mm d^{-1} in the Pacific Northwest where atmospheric transport converges large amounts of moisture. In the southeastern North Pacific, IVT follows an anticyclonic pattern that is associated with the North Pacific High semipermanent pressure center.

The mean moisture transport and precipitation due specifically to identified ARs follow similar patterns and make up substantial fractions (20–70%) of the totals primarily from the southern coast of Japan to the Pacific Northwest (Figure 1b). This pattern is in agreement with the results of Mundhenk *et al.* [2016]. AR precipitation of around $3\text{--}4 \text{ mm d}^{-1}$ extends across the North Pacific. Both AR moisture transport and precipitation are more localized than the totals and in particular are largely absent east of Hawaii and in the northernmost Pacific.

Figure 1c illustrates the relationship between AR IVT and semipermanent pressure patterns in the North Pacific. The layout of the pressure systems dictates the locations of highest AR activity, as AR IVT generally follows isobars and is confined between the Aleutian Low and the North Pacific High. ARs tend to occur to the southeast of upper level troughs, which is reflected in their relationship to the sea level pressure distribution. In the eastern part of the basin, the presence of the Aleutian Low to the northwest and the North Pacific High to the southeast directs southwesterly transport into the continent, creating the southwesterly AR “track” (Figure 1d) and indicating the importance of low-level moisture and winds. By contrast, the climatological storm track (shown in eddy kinetic energy; see supporting information) extends across the entire Pacific and into North America at roughly the same latitude ($\sim 42\text{--}45^\circ$), crossing several isobars of sea level pressure. The strength and positioning of storms are dictated by baroclinic structure [Shaw *et al.*, 2016], and prior idealized climate change simulations have demonstrated that the storm track can shift without affecting the latitude of meridional moisture transport, which is dominated by low-level winds [Caballero and Hanley, 2012]. Therefore, dynamical changes that strongly affect the semipermanent pressure systems likely have a considerable influence on AR moisture transport and precipitation. These may not be as apparent in the storm track, which therefore does not fully represent the sources and trajectory of moisture impacting western North America.

3. LGM Climate From PMIP3 Models and Reconstructions

To understand western North American hydroclimate at the LGM, we turn to the monthly mean climatology output from LGM and preindustrial control (PI) simulations from an ensemble of models participating in the most recent Paleoclimate Modeling Intercomparison Project (PMIP3; Table S1 in the supporting information).

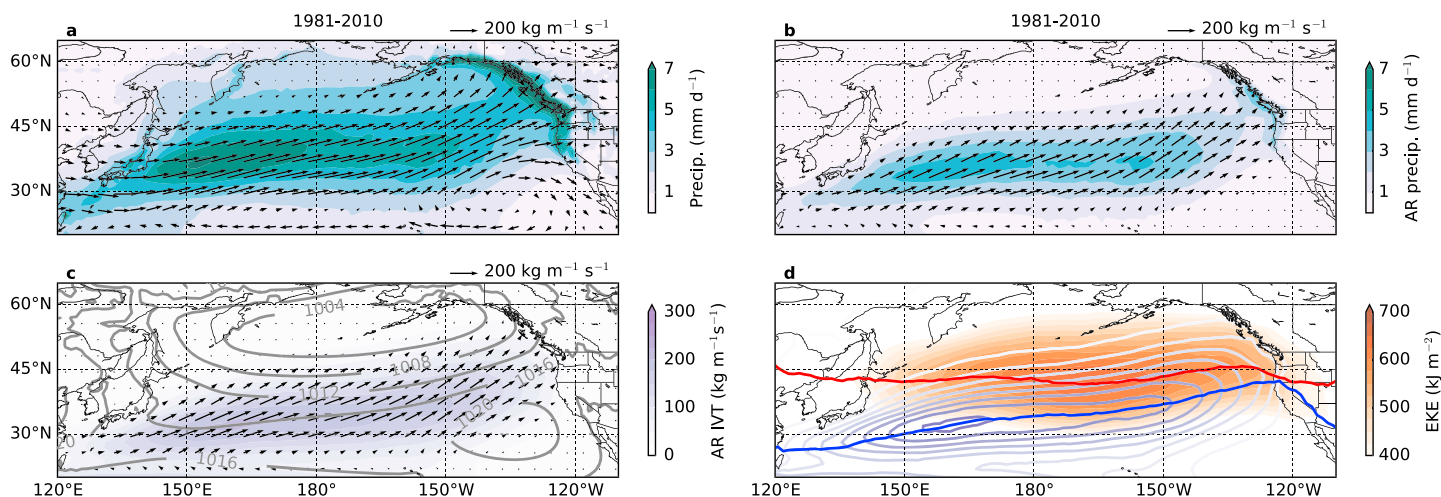


Figure 1. Reanalysis climatology over the North Pacific. (a) Mean October–March integrated vapor transport (IVT) and precipitation from MERRA-2 reanalysis from 1981 to 2010. (b) As in Figure 1a but only for identified atmospheric rivers. (c) Mean integrated vapor transport from atmospheric rivers (AR IVT; colors and arrows) and sea level pressure (gray contours; units hPa). (d) Vertically integrated transient eddy kinetic energy (EKE; see supporting information) from the same data set (filled orange contours), and AR IVT (unfilled blue contours). The mean location of the maximum EKE (roughly the storm track) and the same for the maximum AR IVT are shown by the red and blue lines, respectively. The filled contours in Figure 1c and the unfilled contours in Figure 1d are the same.

The control simulations produce a precipitation distribution over the eastern North Pacific that is in excellent agreement with that from the reanalysis (Figure 2a). At the LGM, the models simulate an enhancement of precipitation on the order of 1 mm d^{-1} between Hawaii and California. Decreases of a similar magnitude occur north of 35°N in the central North Pacific, and larger decreases ($\geq 2 \text{ mm d}^{-1}$) occur in the Pacific Northwest (Figure 2b,c). Given their modern climatology, these changes suggest an important role for ARs, with enhanced AR moisture transport southeast of its present position. The simulations also show precipitation enhancements in southern Nevada, southern Utah, Arizona, and northwestern Mexico of $0.5\text{--}1 \text{ mm d}^{-1}$. In contrast to today, when ARs make landfall preferentially north of 35°N [Dettinger, 2004; Neiman et al., 2008; Rutz et al., 2015], this LGM precipitation distribution implies a southward-shifted coastal crossing, and the accompanying drying of the Pacific Northwest.

A southward shift of the mean landfall latitude of atmospheric moisture transport in the region during the glacial is linked to changes in the pressure systems of the North Pacific. The models simulate a stronger glacial Aleutian Low, and weaker North Pacific High, compared to average modern conditions (Figures 2d and 2e) after accounting for the higher LGM sea level pressure (supporting information). This produces a mean state with generally lower anomalous sea level pressure throughout the eastern North Pacific (Figure 2f), which we interpret as an upstream stationary wave response to the presence of the North American ice sheets and is in agreement with previous simulations that include various LGM ice sheet reconstructions [Bartlein et al., 1998; Otto-Bliesner et al., 2006; Yanase and Abe-Ouchi, 2007; Kim et al., 2008; Lainé et al., 2009]. This in turn implies robust changes in the structure of winds over the North Pacific and the presence of a preferred location for AR formation to the southeast of deepened troughs.

Though their monthly mean output precludes identification of individual ARs, we can diagnose the moisture transport in the PMIP3 models (supporting information). Moisture transport from the model ensemble closely follows isobars of sea level pressure, and the clear relationship between the two again highlights the importance of low-level winds and moisture (Figures 2d–2f). Accompanying the deepened glacial Aleutian Low is westerly IVT that dips farther south in the central Pacific. This shift is most pronounced between 140°W and 160°W , suggesting that high moisture content from the subtropics at these longitudes could more easily be entrained into ARs, potentially as a consequence of southward shifted storms there. In the northeastern Pacific, there is strengthened moisture transport into the southern Alaskan coast at the LGM, in agreement with prior synoptic simulations that show LGM winter storms that track northward along the North American west coast and into Alaska [Unterman et al., 2011], transporting water vapor from lower latitudes. Moisture transport is diverted away from the Pacific Northwest in response to the continental ice sheets, which causes it to flow around this region in a pattern resembling a split upper level jet. In contrast, there is increased southwesterly transport into the North American southwest, where the weakened North Pacific High allows a

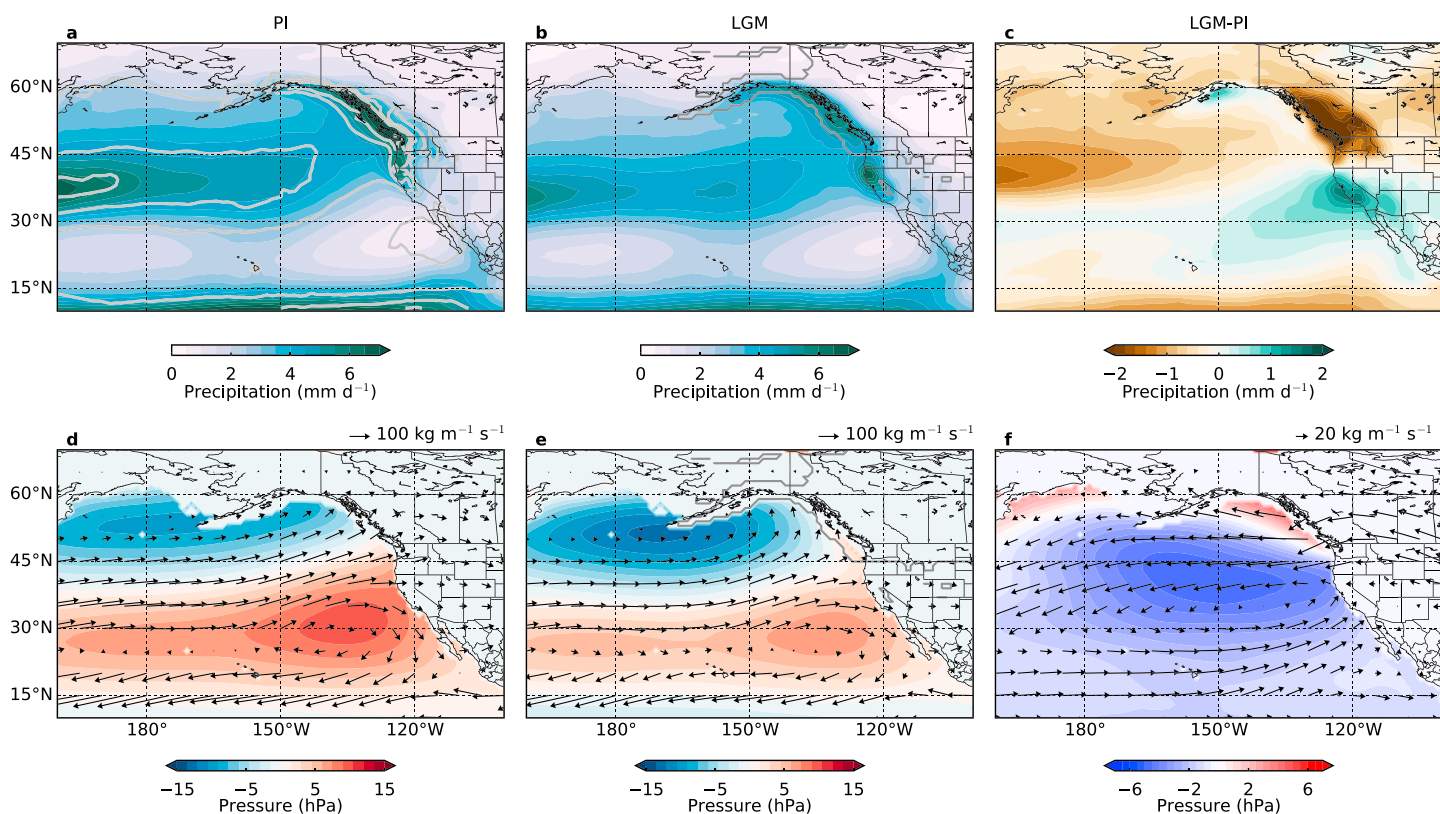


Figure 2. LGM and PI precipitation and moisture transport from PMIP3 ensemble. (a) The model ensemble-mean October–March precipitation for preindustrial control (PI) simulations in the eastern North Pacific and western North America, with reanalysis results overlain in gray contours for comparison (shown contours are 0.5, 2.5, and 4.5 mm d⁻¹). (b) Same as Figure 2a but for the LGM, with approximate outlines of LGM ice sheets in dark gray. (c) The difference between Figures 2b and 2a. (d) Corresponding sea level pressure anomalies (colors) and integrated vapor transport (arrows; see supporting information) for PI simulations. (e) Same as Figure 2d but for the LGM. (f) The differences between Figures 2e and 2d.

substantial increase of moisture transport from around the Hawaiian islands into southern California, suggesting ARs that are shifted to the southeast and routed predominantly into the southwestern coast. At the LGM, southwesterly moisture transport is strengthened just south of locations where precipitation is enhanced over the eastern North Pacific (cf. Figures 2c and 2f), indicative of increased delivery of subtropical moisture. In the North American interior, there is no clear evidence of enhanced northwest-southeast flow, in contrast to findings from previous work [Oster *et al.*, 2015, see supporting information]; instead, there is a north-to-south trend of weaker (easterly in the difference plot) to stronger westerly moisture transport, consistent with a southward shift of landfall locations and enhanced moisture delivery into the southwest of the continent.

Differences between the LGM and PI in both annual-mean and cold-season precipitation in the PMIP3 ensemble produce ~1 mm d⁻¹ enhancements between Hawaii and California and the North American southwest, and decreases elsewhere (Figure 3a). We compare the annual means to a quantitative compilation of reconstructed paleo-precipitation data from western North America (Figure 3b and Table S2). This compilation consists primarily of pollen data [Bartlein *et al.*, 2011], augmented with other quantitative precipitation proxy estimates [Thompson *et al.*, 1999; Lemons *et al.*, 1996; Ibarra *et al.*, 2014; Maher *et al.*, 2014]. The model-data comparison shows general agreement, indicating that the models are able to simulate the magnitude and distribution of changes in moisture delivery to western North America during the LGM. Indeed, the model ensemble and all but one individual models have skill [Hargreaves *et al.*, 2013] (supporting information) in reproducing the available distribution of precipitation differences (Figure 3c), which is dominated by substantial drying of the Pacific Northwest and wetting of the southwest. LGM precipitation enhancements in southern Nevada and Arizona are reproduced in the models, which also simulate considerable enhancements in coastal and southern California precipitation. These patterns imply a southward shift of moisture delivery into the continent that is especially conspicuous in coastal regions where moisture convergence is substantial.

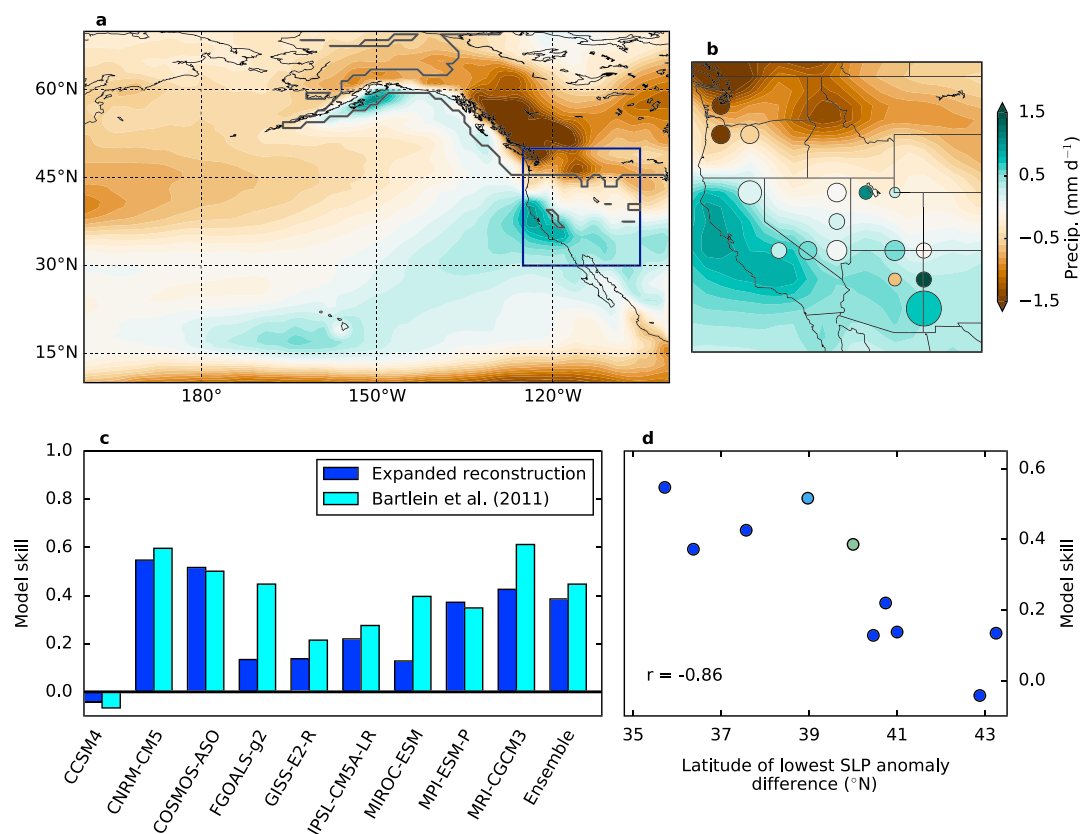


Figure 3. Simulated and reconstructed precipitation. (a) As in Figure 2c, but for the annual mean, with approximate outlines of LGM ice sheets in dark gray. (b) Zoomed-in view of the blue box in Figure 3a, with proxy data shown (filled circles; supporting information). The size of each circle is inversely proportional to the data uncertainty (Table S2). (c) Model skills [Hargreaves et al., 2013] in simulating the proxy distribution of precipitation differences in Figure 2b, with respect to an average difference equal to the mean of the reconstructions. The dark blue is against the expanded reconstruction, while cyan is against the pollen synthesis [Bartlein et al., 2011] exclusively. (d) Correlation between the skill score and the latitude of the lowest simulated sea level pressure anomaly LGM-PI difference between 120° and 150°W in the eastern North Pacific. The correlation coefficient (r) for the nine PMIP3 models is -0.86 , while for the eight models excluding COSMOS-ASO (lighter blue point), it is -0.93 . The green point shows the result for the model ensemble mean.

The PMIP3 models' skill scores against the reconstruction are closely related to their simulated sea level pressure differences between LGM and PI. In particular, the latitude of the lowest LGM-PI sea level pressure difference between 120° and 150°W and the skill score for each model are remarkably anticorrelated (Figure 3d). (Due to its low latitudinal resolution, the COSMOS-ASO model is an outlier among the PMIP3 ensemble (Table S1), and without it the anticorrelation is even stronger.) Increased southwesterly moisture transport and decreased westerly transport into the continent occur south and north, respectively, of the latitude (39°N) of the lowest pressure difference near the coastline (Figure 2f). This latitude is therefore a diagnostic of the magnitude of southward shift of moisture delivery, which dominates the models' predictive accuracy versus the precipitation reconstruction, as indicated by the high correlation with skill score.

4. Atmospheric Rivers in LGM and PI Simulations

Our analysis of the PMIP3 model ensemble suggests an important role for ARs in supporting pluvial conditions in southwestern North America during the LGM. To make this connection explicit, we further analyze daily output from paleoclimate simulations (supporting information) conducted with the LMDZ model [Hourdin et al., 2006, 2013; Dufresne et al., 2013] to resolve individual AR dates and quantify changes in their climatology and distribution between the LGM and the modern climate.

Figure 4a displays the average October–March IVT simulated with the LMDZ model for PI conditions. Compared to the same fields from the reanalysis (Figure 1a), the simulations exhibit a northward bias in

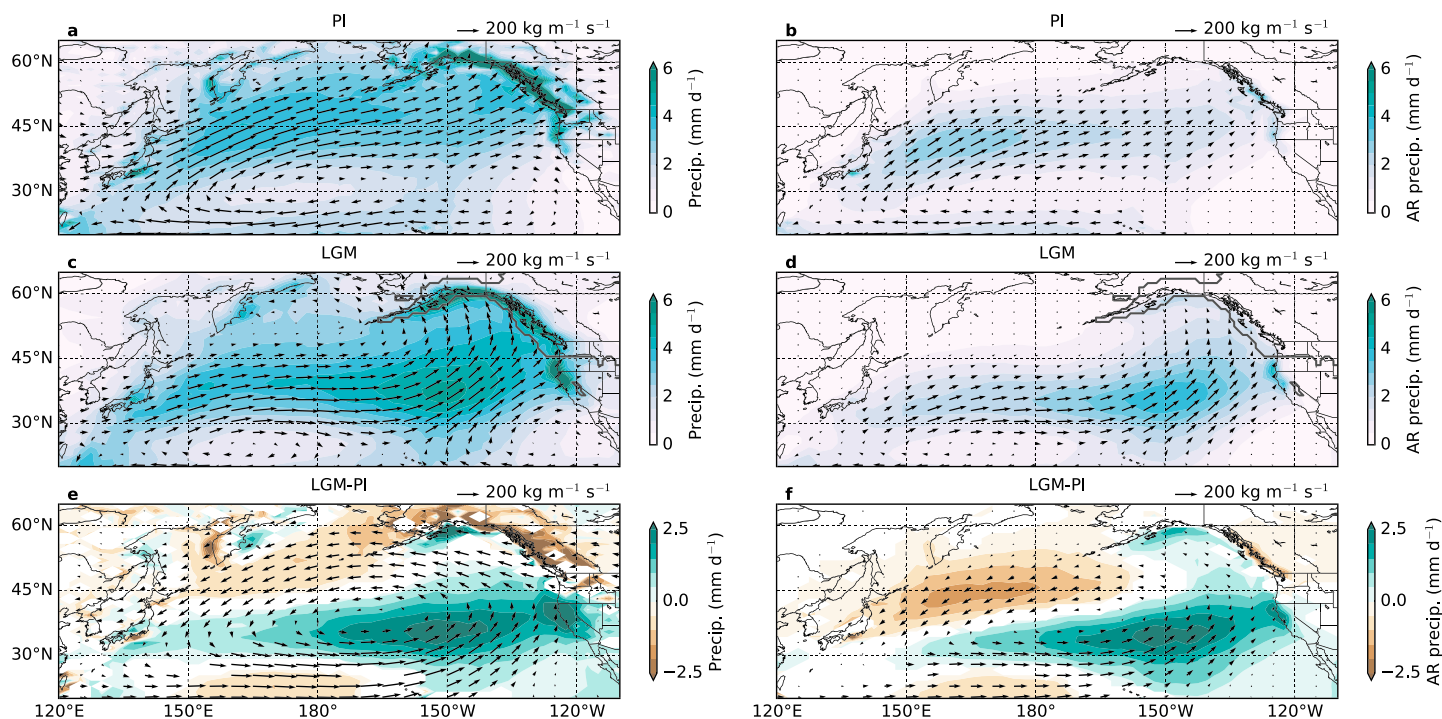


Figure 4. Simulated IVT and atmospheric rivers. (a) Mean October–March IVT and precipitation across the North Pacific for the PI simulation. (b) Mean IVT due solely to ARs (arrows), and associated AR precipitation (colors) for the PI simulation. (c) As in Figure 4a, but for the LGM simulation, with approximate outlines of LGM ice sheets in dark gray. (d) As in Figure 4b, but for the LGM simulation. (e) The differences between Figures 4c and 4a. (f) The differences between Figures 4d and 4b. In Figures 4e and 4f, only areas of significant differences (95% confidence level with a Student’s *t* test) are shown.

the IVT across the Pacific, but the longitudinal layout of the transport is similar, primarily extending from southern Japan to the Pacific Northwest. The highest magnitude ($\sim 300 \text{ kg m}^{-1} \text{ s}^{-1}$) average moisture transport occurs over the western North Pacific, and over the eastern North Pacific, southwesterly IVT is directed toward the coastline. Likewise, including only the IVT and precipitation from identified ARs yields a PI climatology (Figure 4b) that resembles that from reanalysis (Figure 1b), albeit with lower precipitation values around 2–3 mm d^{-1} . Both AR IVT and AR precipitation are more localized than their respective totals and largely absent east of Hawaii and in the northernmost Pacific. Though it is underestimated with respect to the reanalysis, precipitation also strongly peaks in the Pacific Northwest.

The results for the LGM simulations show that the climatological IVT for the winter half year is shifted substantially to the southeast (Figure 4c). In the central North Pacific, the primary band of IVT is approximately 5–10° farther south than in the PI and close to 15° at 150°W. The highest magnitude transport (approximately $300 \text{ kg m}^{-1} \text{ s}^{-1}$) at the LGM also extends across the North Pacific and exhibits a second peak between Hawaii and California where there is little activity in the modern. Between 150° and 180°W, there is also a southward dip in the moisture transport south of 30°N that is largely absent in the PI simulations. As suggested by the PMIP3 results, IVT is strongly diverted away from the Pacific Northwest, and moisture transport in the Gulf of Alaska is southerly and southeasterly into the continent. The decreased moisture transport into the Pacific Northwest indicates the blocking influence of the ice sheets that diverts moisture south, as well as into the Alaskan Peninsula.

The IVT due solely to ARs at the LGM is also shifted southeast, such that mostly westerly transport occurs over much of the western part of the North Pacific, and southwesterly AR IVT occurs between Hawaii and California (Figure 4d). It is noteworthy that total moisture delivery to southwestern North America increases relative to the modern (to around $200 \text{ kg m}^{-1} \text{ s}^{-1}$) due to the southward shifted and intensified AR IVT. AR IVT is also substantially weaker into the Pacific Northwest, and instead, southerly transport increases into the Gulf of Alaska. The North Pacific precipitation pattern due to ARs has a strong maximum of about 3 mm d^{-1} northeast of Hawaii, where ARs converge moisture from the extratropics and the subtropics east of the island chain.

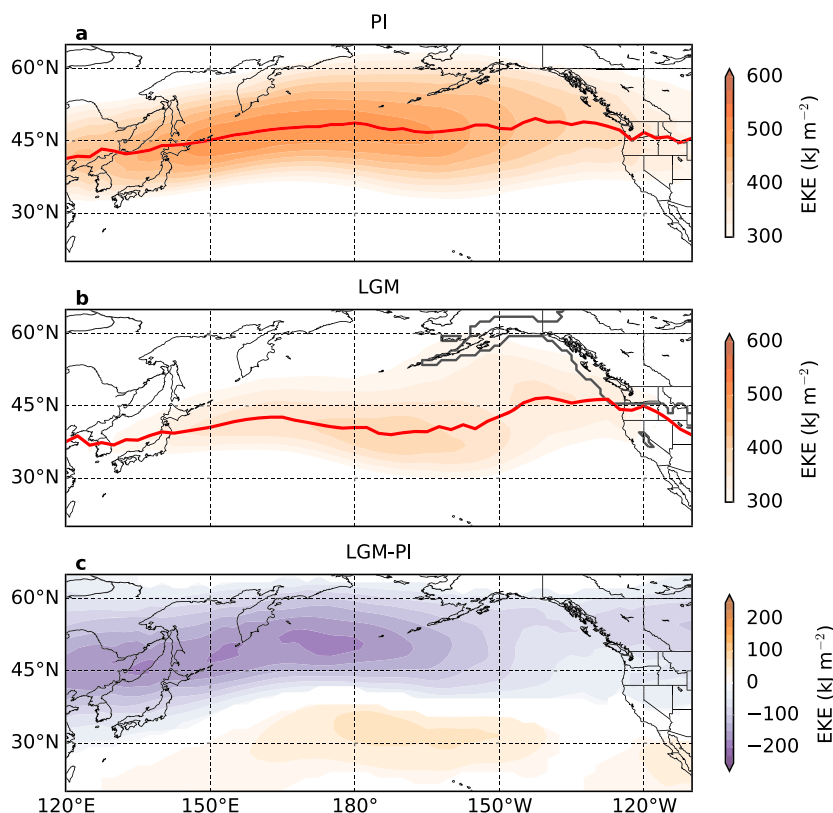


Figure 5. Simulated storm tracks. (a) Mean October–March transient eddy kinetic energy (EKE; supporting information) for the PI simulation, with mean latitude of maxima in red. (b) As in Figure 5a but for the LGM simulation, with approximate outlines of LGM ice sheets in dark gray. (c) The difference between Figures 5b and 5a, showing only areas of significant differences (95% confidence level).

AR precipitation also increases to 2–4 mm d⁻¹ in coastal California. Conversely, there is less precipitation from ARs in the Pacific Northwest, which is now a region where IVT diverges.

In both mean IVT and mean AR IVT, the differences between LGM and PI simulations create a pronounced dipole pattern (Figure 4e), similar to the results from the PMIP3 ensemble (Figures 2c and 2f), highlighting the southeastward shift of transport and precipitation. Decreases in both quantities are strongest over the northwestern North Pacific and are accompanied by increases in the southeastern North Pacific between Hawaii and California. AR precipitation in western North America shows losses of ≥ 1 mm d⁻¹ and gains of ≥ 0.5 mm d⁻¹ in the Pacific Northwest and the southwest, respectively, with higher values in coastal regions. These are comparable (smaller but of similar magnitude) to the precipitation differences simulated by the PMIP3 models and estimated by the proxies (Figure 3b).

Changes in the storm track between LGM and PI in our simulations are significant but less dramatic than those of moisture transport (Figure 5) and consistent with previous findings [e.g., Laine *et al.*, 2009]. The PI simulations exhibit a slight northward bias compared to the reanalysis, consistent with the same in IVT. West of 150°W, the LGM midlatitude band of eddy kinetic energy is shifted south by about 5°. This shift is largest in the central North Pacific, and further supports the possibility of enhanced subtropical moisture entrainment by weather systems from around Hawaii. Closer to North America, latitudinal changes in the position of the storm track are negligible.

In addition to a shift of the storm track, our results also indicate a reduction in storminess over the North Pacific (Figure 5c) despite increased baroclinicity. Similar behavior has been suggested for the glacial North Atlantic [Kageyama and Valdes, 2000; Li and Battisti, 2008; Donohoe and Battisti, 2009]. (We note that single-level eddy kinetic energy results at 500 hPa, as in Merz *et al.* [2015], suggest a southeastward shift but not an obvious reduction of storminess.) On its own, this could be interpreted as implying reduced moisture transport into

North America, but this is not the case. Increased moisture entrainment into ARs from the vicinity of Hawaii increases the atmospheric vapor and precipitation delivered to the southwest of the continent (Figure 4), even under the influence of fewer or less energetic cyclones.

5. Discussion

In the modern, ARs typically weaken after landfall, but some penetrate inland and contribute to heavy precipitation there [Rutz *et al.*, 2014, 2015]. The majority of interior-penetrating ARs occur in the Pacific Northwest, because the majority (~70%) of cold-season landfalling ARs reach the coast north of ~40°N [Rutz *et al.*, 2015]. However, Rutz *et al.* [2015] find that larger fractions (~30–50%) of ARs making landfall along southern California and the Baja Peninsula penetrate inland, because they can pass south of the high Sierras and into the Basin and Range province. If ARs made landfall preferentially south of 35°N during the LGM, as our results would suggest, then a larger total number of ARs would penetrate inland and thereby increase precipitation totals.

Because AR IVT quickly drops over land, the inland-penetrating ARs are difficult to identify with our methods. Therefore, our estimates of mean cold-season precipitation over inland North America should be considered lower bounds. Nevertheless, the simulated LGM-PI precipitation differences are consistent between models and the proxies. Precipitation increases of 0.5–1 mm d⁻¹, accompanied by decreases in total evaporation [Kaufman, 2003], are sufficient to account for reconstructed pluvial conditions from parts of southwestern North America during the LGM.

Acknowledgments

We thank the PMIP3 climate modeling groups listed in Table S1 for making available their model output and the U.S. Department of Energy's PCMDI for distributing it. The MERRA-2 data used in this study are provided by the Global Modeling and Assimilation Office (GMAO) at NASA Goddard Space Flight Center. We thank R. Caballero, J. Mering, A. Kowler, and R. Eagle for helpful discussions of this work. This research was supported by National Science Foundation grants AGS-PRF 1524866 to J.M.L. and CAREER grant EAR-1352212 to A.E.T, as well as "Laboratoire d'Excellence" LabexMER (ANR-10-LABX-19), cofunded by a grant from the French government under the program "Investissements d'Avenir," to A.E.T. LMDZ simulations were performed using HPC resources of IDRIS under the GENCI project 0292. Data presented in this paper that are not publicly available elsewhere are available from the authors upon request.

References

- Bao, J.-W., S. A. Michelson, P. J. Neiman, F. M. Ralph, and J. M. Wilczak (2006), Interpretation of enhanced integrated water vapor bands associated with extratropical cyclones: Their formation and connection to tropical moisture, *Mon. Weather Rev.*, *136*, 1063–1080.
- Bartlein, P. J., K. H. Anderson, P. M. Anderson, M. E. Edwards, C. J. Mock, R. S. Thompson, R. S. Webb, T. Webb III, and C. Whitlock (1998), Paleoclimate simulations for North America over the past 21,000 years: Features of the simulated climate and comparisons with paleoenvironmental data, *Quat. Sci. Rev.*, *49*, 1–10.
- Bartlein, P. J., et al. (2011), Pollen-based continental climate reconstructions at 6 and 21 ka: A global synthesis, *Clim. Dyn.*, *37*, 775–802.
- Benson, L. V., S. P. Lund, J. P. Smoot, D. E. Rhode, R. J. Spencer, K. L. Verosub, L. A. Louderback, C. A. Johnson, R. O. Rye, and R. M. Negrini (2011), The rise and fall of Lake Bonneville between 45 and 10.5 ka, *Quat. Int.*, *235*, 57–69.
- Bromwich, D. H., E. R. Toracinta, H. Wei, R. J. Oglesby, J. L. Fastook, and T. J. Hughes (2004), Polar MM5 simulations of the winter climate of the Laurentide Ice Sheet at the LGM, *J. Clim.*, *17*, 3415–3433.
- Caballero, R., and J. Hanley (2012), Midlatitude eddies, storm-track diffusivity, and poleward moisture transport in warm climates, *J. Atmos. Sci.*, *69*, 3237–3250.
- COHMAP Members (1988), Climatic changes of the last 18,000 years: Observations and model simulations, *Science*, *241*, 1043–1052.
- Cordeira, J. M., F. M. Ralph, and B. J. Moore (2013), The development and evolution of two atmospheric rivers in proximity to western North Pacific tropical cyclones in October 2010, *Mon. Weather Rev.*, *141*, 4234–4255.
- Dacre, H. F., P. A. Clark, O. Martinez-Alvarado, M. A. Stringer, and D. A. Lavers (2015), How do atmospheric rivers form?, *Bull. Am. Meteorol. Soc.*, *96*, 1243–1255.
- Dettinger, M. (2004), Fifty-two years of "pineapple-express" storms across the West Coast of North America, Tech. Rep. CEC-500-2005-004, California Energy Commission PIER Energy-Related Environmental Research Report, California Energy Commission, Sacramento, Calif.
- Dettinger, M. D., F. M. Ralph, T. Das, P. J. Neiman, and D. R. Cayan (2011), Atmospheric rivers, floods and the water resources of California, *Water*, *3*, 445–478.
- Donohoe, A., and D. S. Battisti (2009), Causes of reduced North Atlantic storm activity in a CAM3 simulation of the Last Glacial Maximum, *J. Clim.*, *22*, 4793–4808.
- Dufresne, J.-L., et al. (2013), Climate change projections using the IPSL-CM5 Earth System Model: From CMIP3 to CMIP5, *Clim. Dyn.*, *40*, 2123–2165.
- Guan, B., N. P. Molotch, D. E. Waliser, E. J. Fetzer, and P. J. Neiman (2010), Extreme snowfall events linked to atmospheric rivers and surface air temperature via satellite measurements, *Geophys. Res. Lett.*, *37*, L20401, doi:10.1029/2010GL044696.
- Hargreaves, J. C., J. D. Annan, R. Ohgaito, A. Paul, and A. Abe-Ouchi (2013), Skill and reliability of climate model ensembles at the Last Glacial Maximum and mid-Holocene, *Clim. Past*, *9*, 811–823.
- Hendy, I. L., T. J. Napier, and A. Schimmelmann (2015), From extreme rainfall to drought: 250 years of annually resolved sediment deposition in Santa Barbara Basin, California, *Quat. Int.*, *387*, 3–12.
- Hostetler, S., and L. V. Benson (1990), Paleoclimatic implications of the high stand of Lake Lahontan derived from models of evaporation and lake level, *Clim. Dyn.*, *4*, 207–217.
- Hourdin, F., et al. (2006), The LMDZ4 general circulation model: Climate performance and sensitivity to parameterized physics with emphasis on tropical convection, *Clim. Dyn.*, *27*, 787–813.
- Hourdin, F., et al. (2013), Impact of the LMDZ atmospheric grid configuration on the climate and sensitivity of the IPSL-CM5A coupled model, *Clim. Dyn.*, *40*, 2167–2192.
- Ibarra, D. E., A. E. Egger, K. L. Weaver, C. R. Harris, and K. Maher (2014), Rise and fall of late Pleistocene pluvial lakes in response to reduced evaporation and precipitation: Evidence from Lake Surprise, California, *GSA Bull.*, *11–12*, 1387–1415, doi:10.1007/s00382-014-2162-0.
- Kageyama, M., and P. J. Valdes (2000), Impact of the North American ice-sheet orography on the Last Glacial Maximum eddies and snowfall, *Geophys. Res. Lett.*, *27*, 1515–1518.
- Kaufman, D. S. (2003), Amino acid paleothermometry of Quaternary ostracodes from the Bonneville Basin, Utah, *Quat. Sci. Rev.*, *22*, 899–914.

- Kim, S.-J., T. J. Crowley, D. J. Erickson, B. Govindasamy, P. B. Duffy, and B. Y. Lee (2008), High-resolution climate simulation of the Last Glacial Maximum, *Clim. Dyn.*, *31*, 1–16.
- Kirby, M. E., S. J. Feakins, N. Bonuso, J. M. Fantozzi, and C. A. Hiner (2013), Latest Pleistocene to Holocene hydroclimates from Lake Elsinore, California, *Quat. Sci. Rev.*, *76*, 1–15.
- Knipperz, P., and H. Wernli (2010), A Lagrangian climatology of tropical moisture exports to the Northern Hemisphere extratropics, *J. Clim.*, *23*, 987–1003.
- Kutzbach, J. E., and H. E. Wright (1985), Simulation of the climate of 18,000 yr BP: Results for the North American/North Atlantic/European sector and comparison with the geologic record, *Quat. Sci. Rev.*, *4*, 147–187.
- Lachniet, M. S., R. F. Denniston, Y. Asmerom, and V. J. Polyak (2014), Orbital control of western North America atmospheric circulation and climate over two glacial cycles, *Nat. Commun.*, *5*, 3805.
- Lainé, A., M. Kageyama, D. Salas-Méliea, A. Voldoire, G. Rivière, G. Ramstein, S. Planton, S. Tyteca, and J. Y. Peterschmitt (2009), Northern Hemisphere storm tracks during the Last Glacial Maximum in the PMIP2 ocean-atmosphere coupled models: Energetic study, seasonal cycle, precipitation, *Clim. Dyn.*, *32*, 593–614.
- Lemons, D. R., M. R. Milligan, and M. A. Chan (1996), Paleoclimatic implications of late Pleistocene sediment yield rates for the Bonneville Basin, northern Utah, *Palaeogeogr. Palaeoclimatol. Palaeoecol.*, *123*, 147–159.
- Li, C., and D. S. Battisti (2008), Reduced Atlantic storminess during the Last Glacial Maximum: Evidence from a coupled climate model, *J. Clim.*, *21*, 3561–3579.
- Lyle, M., L. Heusser, C. Ravelo, M. Yamamoto, J. Barron, N. S. Diffenbaugh, T. Herbert, and D. Andreasen (2012), Out of the tropics: The Pacific, Great Basin lakes, and late Pleistocene water cycle in the western United States, *Science*, *337*, 1629–1633.
- Maher, K., D. E. Ibarra, J. L. Oster, D. M. Miller, J. L. Redwine, M. C. Reheis, and J. W. Harden (2014), Uranium isotopes in soils as a proxy for past infiltration and precipitation across the western United States, *Am. J. Sci.*, *314*, 821–857.
- Manabe, S., and A. J. Broccoli (1985), The influence of continental ice sheets on the climate of the Ice Age, *J. Geophys. Res.*, *90*, 2167–2190.
- Merz, N., C. C. Raible, and T. Woollings (2015), North Atlantic eddy-driven jet in interglacial and glacial winter climates, *J. Clim.*, *28*, 3977–3997.
- Mundhenk, B. D., E. A. Barnes, and E. D. Maloney (2016), All-season climatology and variability of atmospheric river frequencies over the North Pacific, *J. Clim.*, *29*, 4885–4903.
- Neiman, P. J., F. M. Ralph, G. A. Wick, J. D. Lundquist, and M. D. Dettinger (2008), Meteorological characteristics and overland precipitation impacts of atmospheric rivers affecting the West Coast of North America based on eight years of SSM/I satellite observations, *J. Hydrometeorol.*, *9*, 22–47.
- Oster, J. L., D. E. Ibarra, M. J. Winnick, and K. Maher (2015), Steering of westerly storms over western North America at the Last Glacial Maximum, *Nat. Geosci.*, *8*, 201–205.
- Otto-Bliesner, B. L., E. C. Brady, G. Clauzet, R. Tomas, S. Levis, and Z. Kothavala (2006), Last Glacial Maximum and Holocene climate in CCSM3, *J. Clim.*, *19*, 2526–2544.
- Oviatt, C. G., R. S. Thompson, D. S. Kaufman, J. Bright, and R. M. Forester (1999), Reinterpretation of the Burmester Core, Bonneville Basin, Utah, *Quat. Res.*, *52*, 180–184.
- Owen, L. A., R. C. Finkel, R. A. Minnick, and A. E. Perez (2003), Extreme southwestern margin of late Quaternary glaciation in North America: Timing and controls, *Geology*, *31*, 729–732.
- Payne, A. E., and G. Magnusdottir (2014), Dynamics of landfalling atmospheric rivers over the North Pacific in 30 years of MERRA reanalysis, *J. Clim.*, *27*, 7133–7150.
- Ralph, F. M., P. J. Neiman, and R. Rotunno (2005), Dropsonde observations in low-level jets over the Northeastern Pacific Ocean from CALJET-1998 and PACJET-2001: Mean vertical-profile and atmospheric-river characteristics, *Mon. Weather Rev.*, *133*, 889–910.
- Ralph, F. M., P. J. Neiman, G. A. Wick, S. I. Gutman, M. D. Dettinger, D. R. Cayan, and A. B. White (2006), Flooding on California's Russian River: Role of atmospheric rivers, *Geophys. Res. Lett.*, *33*, L13801, doi:10.1029/2006GL026689.
- Ralph, F. M., P. J. Neiman, G. N. Kiladis, K. Weickmann, and D. W. Reynolds (2011), A multiscale observational case study of a Pacific atmospheric river exhibiting tropical–extratropical connections and a mesoscale frontal wave, *Mon. Weather Rev.*, *139*, 1169–1189.
- Reheis, M. C., J. Bright, S. P. Lund, D. M. Miller, G. Skipp, and R. J. Fleck (2012), A half-million-year record of paleoclimate from the Lake Manix Core, Mojave Desert, California, *Palaeogeogr. Palaeoclimatol. Palaeoecol.*, *365*, 11–37.
- Rutz, J. J., and W. J. Steenburgh (2012), Quantifying the role of atmospheric rivers in the interior western United States, *Atmos. Sci. Lett.*, *13*, 257–261.
- Rutz, J. J., W. J. Steenburgh, and F. M. Ralph (2014), Climatological characteristics of atmospheric rivers and their inland penetration over the western United States, *Mon. Weather Rev.*, *142*, 905–921.
- Rutz, J. J., W. J. Steenburgh, and F. M. Ralph (2015), The inland penetration of atmospheric rivers over western North America: A Lagrangian analysis, *Mon. Weather Rev.*, *143*, 1924–1944.
- Shaw, T. A., et al. (2016), Storm track processes and the opposing influences of climate change, *Nat. Geosci.*, *9*, 656–664.
- Sodemann, H., and A. Stohl (2013), Moisture origin and meridional transport in atmospheric rivers and their association with multiple cyclones, *Mon. Weather Rev.*, *141*, 2850–2868.
- Thompson, R. S., K. H. Anderson, and P. J. Bartlein (1999), Quantitative paleoclimatic reconstructions from late Pleistocene plant macrofossils of the Yucca Mountain region, U.S. Geol. Surv. Open File Rep. 99-338, U.S. Dept. of the Inter., U.S. Geol. Surv., Denver, Colo.
- Unterman, M. B., T. J. Crowley, K. I. Hedges, S.-J. Kim, and D. J. Erickson (2011), Paleometeorology: High resolution Northern Hemisphere wintertime mid-latitude dynamics during the Last Glacial Maximum, *Geophys. Res. Lett.*, *38*, L23702, doi:10.1029/2011GL049599.
- Wagner, J. D. M., J. E. Cole, J. W. Beck, P. J. Patchett, G. M. Henderson, and H. R. Barnett (2010), Moisture variability in the southwestern United States linked to abrupt glacial climate change, *Nat. Geosci.*, *3*, 110–113.
- Yanase, W., and A. Abe-Ouchi (2007), The LGM surface climate and atmospheric circulation over East Asia and the North Pacific in the PMIP2 coupled model simulations, *Clim. Past*, *3*, 439–451.
- Zhu, Y., and R. E. Newell (1998), A proposed algorithm for moisture fluxes from atmospheric rivers, *Mon. Weather Rev.*, *21*, 152–158.